Mechanism of Inhibition of the V-Type Molecular Motor by Tributyltin Chloride

Mizuho Takeda,[†] Chiyo Suno-Ikeda,[‡] Katsuya Shimabukuro,[§] Masasuke Yoshida,[†¶] and Ken Yokoyama[†¶*]
[†]Chemical Resources Laboratory, Tokyo Institute of Technology, Yokohama, Japan; [‡]Human Receptor Crystallography Project, Exploratory Research for Advanced Technology, Japan Science and Technology Agency, Kyoto, Japan; [§]Department of Biological Science, Florida State University, Tallahassee, Florida; and [¶]ATP-Synthesis Regulation Project, International Cooperative Project, Japan Science and Technology Agency, National Museum of Emerging Science and Innovation, Tokyo, Japan

ABSTRACT Tributyltin chloride (TBT-Cl) is an endocrine disruptor found in many animal species, and it is also known to be an inhibitor for the V-ATPases that are emerging as potential targets in the treatment of diseases such as osteoporosis and cancer. We demonstrated by using biochemical and single-molecular imaging techniques that TBT-Cl arrests an elementary step for rotary catalysis of the V_1 motor domain. In the presence of TBT-Cl, the consecutive rotation of V_1 paused for a long duration (~0.5 s), even at saturated ATP concentrations, and the pausing positions were localized at 120° intervals. Analysis of both the pausing time and moving time revealed that TBT-Cl has little effect on the binding affinity for ATP, but, rather, it arrests the catalytic event(s). This is the first report to demonstrate that an inhibitor arrests an elementary step for rotary catalysis of a V-type ATP-driven rotary motor.

INTRODUCTION

Tributyltin chloride (TBT-Cl) has been used widely as an antiseptic, especially as a disinfecting agent on ships. This practice has caused severe contamination of the aquatic ecosystem (1). TBT-Cl is also known to be an endocrine disruptor in many animal species, and it produces a wide range of irritant and toxic effects on mammals (2). However, the precise mechanism of toxicity of TBT-Cl is not well understood.

Vacuolar type ATPases (V-ATPases), which function in a variety of physiologic processes (3), have been reported as targets of TBT-Cl (4–6). In eukaryotic cells, V-ATPases reside within the membranes of intracellular compartments that include endosomes, lysosomes, and secretory vesicles, and within plasma membranes of certain cells, such as osteoclasts. The eukaryotic V-ATPases couple ATP hydrolysis to transmembrane proton translocation. The related enzymes of eukaryotic V-ATPases were found in some bacteria. These prokaryotic V-ATPases function as either ATP synthases or as sodium pumps (7,8).

The V-ATPases are related to the F-type ATP synthase (F-ATPase) in that they are comprised of membrane-embedded subunits, wherein V_o is equivalent to F_o, complexed with peripheral subunits, wherein V_1 is equivalent to F_1 (3). Similarly to the F-ATPase holoenzyme, the V-ATPase holoenzyme couples ATP hydrolysis by V_1 to ion translocation through V_o, using a rotary mechanism (9,10).

The prokaryotic V-type ATPase/synthases from a thermophilic eubacterium, *Thermus thermophilus* (*T. thermophilus*), have a simpler subunit composition than that of eukaryotic V-ATPases (11,12). The hydrophilic V_1 domain of *T. thermophilus* is an ATPase made up of four kinds of subunits with $A_3B_3D_1F_1$ stoichiometry. The catalytic A and B subunits in V_1 show an apparent sequence similarity to the β and α subunits of F_1, respectively (13). In contrast, the D and F subunits, which constitute a rotor shaft in V_1 (9), show no sequence homology to either the γ or ε subunit of F_1. Unlike the isolated V_o domain of eukaryotic V-ATPases, the V_o domain isolated from *T. thermophilus* has proton permeability (14).

It has been shown that the macrolide antibiotics bafilomycin A_1 and concanamycin specifically inhibit proton pump activity of eukaryotic V-ATPases (15). Treatment of cells with these antibiotics has been shown to inhibit physiologic processes such as autophagy and Bax-dependent apoptosis (16), as well as cell proliferation (17). From genetic studies using yeasts, Wang et al. found that subunit a, which is a part of the proton channel in V_o, participates in bafilomycin binding (18). Loss of V-ATPase activity in cells affects several physiologic processes, and therefore, V-ATPases can be very useful in drug development. Thus, it is important to investigate inhibitory mechanisms of V-ATPase inhibitors in detail.

Ballmoos et al. (19) reported that subunit a in F_o of bacterial ATP synthase is specifically labeled upon photo-inactivation with an aryldiazirine derivative of TBT-Cl. In contrast, ATPase activity of isolated F_1 is not inhibited by TBT-Cl (20). In the case of V-ATPases, subunits in V_1 and V_o have been reported to be targets of different organotin inhibitors. Irradiation of the V-ATPase in bovine adrenal chromaffin granules with a radioactive organotin photo-affinity analog led to labeling of catalytic subunit A in the V-ATPase (5). In contrast, organotin flavone complexes were found to interact with the 16 k-Da proteolipid subunit in V_o of the *Nephrops noevegicus* V-ATPase (4).

Submitted February 27, 2008, and accepted for publication October 9, 2008.

*Correspondence: yokoyama.k.ab@m.titech.ac.jp

Editor: David D Hackney.

0006-3495/09/02/1210/8 $2.00

doi: 10.1016/j.bpj.2008.10.031

In this study, we report the detailed inhibitory effects of TBT-Cl on the *T. thermophilus* V-ATPase using both bulk-phase and single-molecule analysis. From this analysis, we propose a mechanism for inhibition of rotational catalysis in V_1 by utilization of TBT-Cl.

MATERIALS AND METHODS

Protein preparation

A mutant $A_{(His\text{-}8/C28S/S232A/T235S/C508S)3}B_{(C264S)3}D_{(E48C/Q55C)}F$ (V_1) and the subcomplex $A_{(His\text{-}8/C28S/S232A/T235S/C508S)3}B_{(C264S)3}D_{(E48C/Q55C)}$ ($V_1\Delta F$) derived from *T. thermophilus* were expressed and purified as described previously (21). For single-molecule experiments, the V_1 and $V_1\Delta F$ were biotinylated at two cysteines located in subunit D by incubation with three-fold molar excess of *N*-6-(Biotinylamino)hexanoyl-*N*′-[2-(*N*-maleimido)ethyl]piperazine, hydrochloride (Dojindo) for 1 h at room temperature. Unreacted reagents were removed with NAP5-column (GE Healthcare, Buckinghamshire, UK), and the biotinylated proteins were immediately frozen with liquid nitrogen and stored at −80°C. V-ATPase (V_oV_1 holenzyme) and V_o of *T. thermophilus* were purified as described previously (14). Protein concentrations were determined with the BCA protein assay (Pierce) for V_oV_1 and V_o, and absorbance at 280 nm was calibrated by quantitative amino acid analysis for V_1 (22). The subcomplex of F_1 ($\alpha_3\beta_3\gamma$), termed F_1 unless otherwise noted, was purified as described (23).

Bulk-phase measurements of ATPase activity

The ATPase activity of V_1, $V_1\Delta F$, V-ATPase holoenzyme, and F_1 were determined with an ATP-regenerating system (0.2 mM reduced form of nicotinamide adenine dinucleotide, 0.1 mg/ml pyruvate kinase, 0.1 mg/ml lactate dehydrogenase, and 2 mM phosphoenolpyruvate) in solution R (50 mM Tris-HCl (pH 8.0), 100 mM KCl, 2 mM $MgCl_2$ ($\leq$2 mM ATP), and equimolar $MgCl_2$ with >2 mM ATP were contained for V_1) at 25°C. 0.05% *n*-Dodecyl-β-D-maltoside was added to measure the ATPase activity of the V-ATPase holoenzyme.

Measurements of proton permeability of V_o-liposomes

Membrane vesicles (44 mg/ml) pretreated with phospholipid (soybean L-α-phosphatidylcholine, type II-S, Sigma Chemical, St. Louis, MO) were suspended in solution A (10 mM HEPES/KOH, pH 7.5, 5 mM $MgSO_4$, 10% glycerol) and sonicated for 5 min at 4°C, and 20 μl of V_o solution (5 mg/ml) was added to 180 μl of the suspension. The mixture was gently stirred, then frozen with liquid nitrogen and thawed at room temperature. For loading with potassium ion, the V_o-liposome was pelleted by centrifugation (200,000 × *g*, 20 min, 4°C) and incubated with 200 μl of 0.25 M potassium gluconate at 50°C for 30 min. For measurement purposes, the potassium-loaded V_o-liposome was pelleted by centrifugation (200,000 × *g*, 20 min, 4°C) and resuspended in solution B (10 mM HEPES/NaOH, pH 7.5, 5 mM $MgSO_4$, 0.25 M sucrose). Proton permeability was measured as described previously (11). The various concentrations of TBT-Cl were preincubated with V_o-liposome suspension for 1 h at 4°C. The initial assay mixture contained 50 μg/ml proteoliposome and 0.2 μM 9-amino-6-chloro-2-methoxyacridine in solution B, and the reactions were initiated by injecting 20 μM valinomycin. The assays were carried out at 40°C. 0.1 μM carbonylcyanide *p*-trifluoromethoxyphenylhydrazone was added at the end of assays to check the extent of 9-amino-6-chloro-2-methoxyacridine quenching.

Single-molecule analysis

We measured the ATPase activity of V_1 by observing rotating beads attached to the D subunit surrounded by the A_3B_3 ring, which was fixed on a Ni^{2+}-NTA-modified cover glass by His-tags. A flow chamber was assembled from the cover glass (objective side) and a slide glass with two spacers of 50-μm thickness. The inner glass surface was coated with bovine serum albumin (Sigma) by infusion of solution R containing 2 mg/ml bovine serum albumin to avoid nonspecific interaction. 20 μl of biotinylated enzyme (50 nM in solution R) was infused to the chamber. After 5 min of incubation, 0.03% streptavidin-coated beads (φ = 209 nm, Polyscience, Warrington, PA) in solution R were infused and incubated for 8 min to attach the bead to enzyme. Observation of rotation was initiated by infusing the solution R that contained the indicated concentrations of ATP and TBT-Cl and the solution R was supplemented with the ATP-regenerating system. All procedures were done after washing the chamber with solution R. Rotating duplex beads were observed with a dark-field microscope (IX-70; Olympus, Tokyo, Japan) with a dark-field condenser (numerical apertures 1.2–1.4, Olympus) and a ×100 objective (numerical apertures 0.5–1.35, Olympus). The images of rotating beads were recorded with a 1- or 2-ms time resolution as an 8-bit Audio Video Interleave file with a complementary metal oxide semiconductor high-speed camera (Hi-DcamII, NAC Image Technology, Tokyo, Japan). Custom software (created by Ryohei Yasuda and Kengo Adachi, affiliated with Japan Science and Technology Agency) was used for analyses of the bead movements and dwelling times of steps. Time-averaged rotation speed was calculated from >10 consecutive revolutions. All experiments were done at 25°C.

RESULTS

Effects of TBT-Cl inhibition on V_1 and V_o domains

We investigated the effects of TBT-Cl on the ATPase activity of both the V-ATPase holoenzyme and resolved V_1 of *T. thermophilus* by bulk-phase analysis. In this study, the mutant enzymes, which were found to be resistant to ADP-Mg inhibition, were used for the ATPase assay. The properties for ATPase activity of the mutated enzymes were basically similar to those of the wild-type enzymes (21,22). The F_1 from thermophilic *Bacillus* PS3 was also analyzed as a control. As shown in Fig. 1 *A*, TBT-Cl did not inhibit the ATPase activity of F_1 at μM concentrations, consistent with the previous report (20). In contrast, the ATPase activity of V_1 was efficiently inhibited as the TBT-Cl concentration increased. The estimated K_i value for TBT-Cl inhibition was 11.6 ± 0.7 μM (mean ± SE) (Fig. 1 *A, red curve*). These results indicate that, unlike F_1, TBT-Cl inhibits the ATPase activity of V_1. TBT-Cl also inhibited the ATPase activity of the V-ATPase holoenzyme; however, the K_i value was apparently lower than that for V_1. To examine the effects of TBT-Cl on the V_o domain alone, the V_o domain was reconstituted into potassium-loaded liposomes, and proton permeability was measured. To prepare potassium-loaded V_o-liposomes, potassium gluconate, rather than potassium chloride, was used, because TBT-Cl alone is known to promote Cl^-/H^+ symport activity in liposomes (24). The V_o-liposomes preincubated with the various concentrations of TBT-Cl were subjected to the proton permeability experiments. As shown in Fig. 1 *B*, the untreated V_o-liposomes showed apparent proton permeability. However, after incubation with TBT-Cl, the V_o-liposomes exhibited weaker proton permeability in a dose-dependent manner. The proton permeability of the V_o-liposome was completely abolished by the preincubation

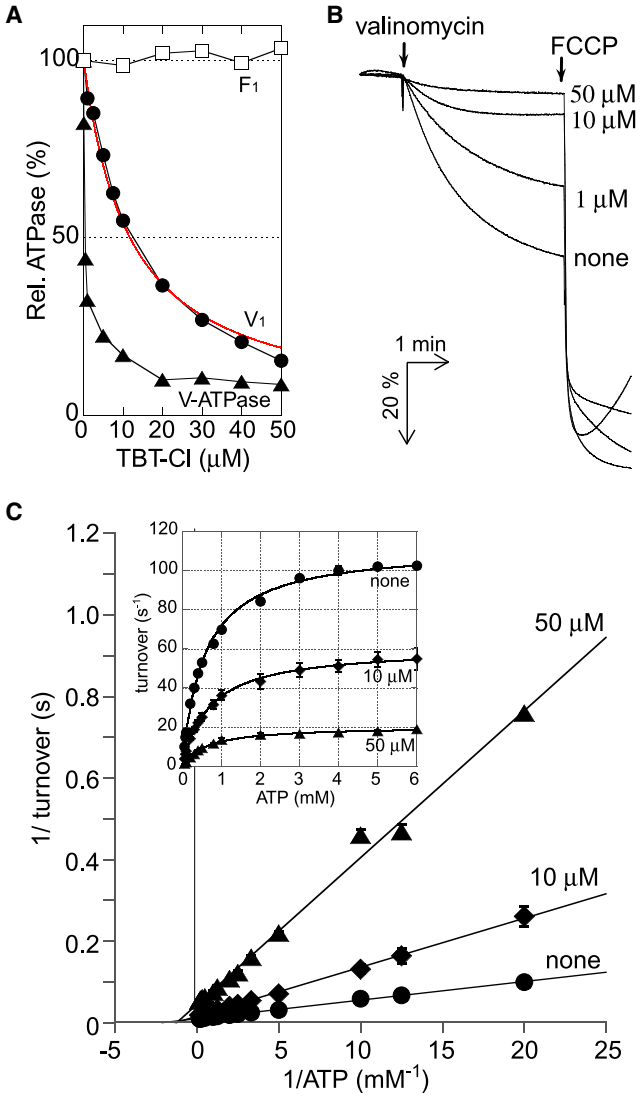

FIGURE 1 Bulk- phase analysis for effects of TBT-Cl on V-ATPase. (*A*) The ATPase activities of V_1 (●), V-ATPase holoenzyme (▲), and F_1 (□) at 4 mM (V_1 and V-ATPase holoenzyme) or 2 mM (F_1) ATP in the presence of indicated concentrations of TBT-Cl. The K_i value TBT-Cl for inhibition of V_1 ATPase activity by TBT-Cl was estimated to be 11.6 ± 0.7 μM by fitting data to the equation $v = V_{max}[S]/(K_m + [S])(1 + [I]/K_i)$ (*red line*). The ATPase activities were calculated using averaged values from two or three measurements. (*B*) Proton permeability of V_o-liposomes in the presence of indicated concentrations of TBT-Cl. The reaction was started by addition of valinomycin, and terminated by injection of FCCP. (*C*) Lineweaver-Burk plots representing reciprocal of the V_1 ATPase activity versus reciprocal of ATP concentrations in the presence of 50 μM (▲), 10 μM (◆), and no TBT-Cl (●). The plots are fitted by linear regression on full data sets. (*Inset*) [S]-*v* plots derived from the Lineweaver-Burk plots. The lines show fitting functions with $V_{max} = 21.1 \pm 0.5\ s^{-1}$ and $K_m = 628 \pm 12$ μM (50 μM), $V_{max} = 60.9 \pm 5.0\ s^{-1}$ and $K_m = 704 \pm 46$ μM (10 μM), and $V_{max} = 112.0 \pm 0.3\ s^{-1}$ and $K_m = 560 \pm 15$ μM (no TBT-Cl), respectively. Each point represents mean ± SE of three measurements.

with 50 μM TBT-Cl. These results indicate that TBT-Cl interacts with the V_o domain and blocks proton translocation through the V_o domain, suggesting that TBT-Cl affects both the V_1 and the V_o domains.

Bulk phase kinetics for TBT-Cl inhibition of V_1

To analyze the ways in which TBT-Cl inhibited V_1, we measured steady-state ATPase activity of V_1 at different concentrations of TBT-Cl. Fig. 1 *C* shows Lineweaver-Burk plots in the presence of the indicated concentrations of TBT-Cl. The plots portray the graphic consequences of noncompetitive inhibition, and the ATPase activity obeyed simple Michaelis-Menten kinetics (Fig. 1 *C, inset*). Apparent K_m and V_{max} values were deduced by analysis of the plots. The V_{max} was decreased from 112.0 ± 0.3 s^{-1} (no TBT-Cl) to 60.9 ± 5.0 s^{-1} (10 μM TBT-Cl) and 21.1 ± 0.5 s^{-1} (50 μM TBT-Cl) (mean ± SE) without any appreciable change of K_m, suggesting that TBT-Cl acts in a noncompetitive fashion. In addition, the ATPase activity of V_1 was mostly restored after the TBT-Cl-inhibited enzyme was applied to a gel filtration column (data not shown). These results indicate that TBT-Cl interacts with V_1 noncovalently.

Rotation of V_1 in the presence of TBT-Cl under V_{max} conditions

We analyzed the inhibition mechanism of V_1 by TBT-Cl using the single-molecule technique. The rotation of 209 nm duplex bead attached to the D subunit surrounded by the A_3B_3 ring was recorded with a high-speed camera, which enabled us to observe the rotation of V_1 at high time resolution. At 4 mM ATP in the absence of TBT-Cl, the bead rotated continuously (Fig. 2 *A, black line*), and the maximum rotation speed was calculated to be 19.7 ± 2.9 Hz (mean ± SE, 5 molecules). The rate was about one half of the rate calculated from the bulk-phase activity (37.3 Hz = 112.0 s^{-1} /3), most likely due to the impelled frictional load on the beads attached to the rotor shaft (25). Although the rotation at 4 mM ATP seemed smooth, it was frequently interrupted with undefined short pauses (Fig. S1 *A* in the Supporting Material), which is not obvious at video time resolution (33 ms). The distribution of this pausing time showed a single exponential decay, and the fit with a single exponential gave a time constant of 0.02 ± 0.00 s (mean ± SE) (Fig. S1 *B*). The average occurrence of the pauses was 0.9 per revolution, and >96.4% of these duration times were ≤0.2 s. The cause of these short pauses has not been determined. Hirono-Hara et al. reported similar undetermined short pauses observed in F_1 (26).

In the presence of TBT-Cl, in addition to the undefined short pauses, long pauses were frequently observed (Fig. 2, *A–C*) and the rotation rate was dramatically decreased. The histogram of all pauses that were observed in the presence of 10 μM TBT-Cl could not be fitted with a simple single exponential, but it was fitted well with a sum of two exponentials using an adequate time bin-width. This suggests that the two pauses represent at least two different molecular events. The histogram of the short pause was well fitted with a single exponential, but it was not fitted with a sum of two exponentials by small time bin-width (0.02 s). At the long time region of the histogram by the bin size, the frequency was very low,

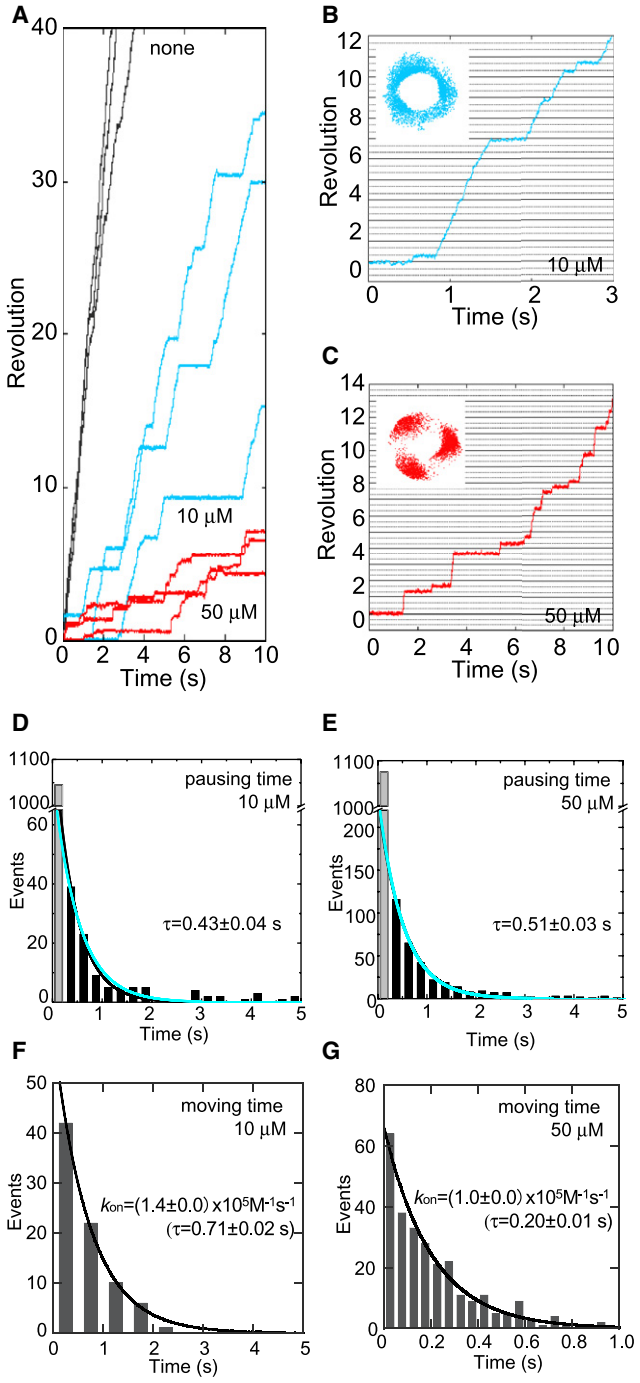

FIGURE 2 Effect of TBT-Cl on the rotation of V_1 at saturating ATP concentration. (*A*) Time course of the rotation within V_1 at 4 mM ATP in the presence of 50 μM (*red line*) and 10 μM (*blue line*) TBT-Cl, and in the absence of TBT-Cl (*black line*). (*B* and *C*) Expanded time courses of rotation in the presence of 10 μM (*B*) and 50 μM (*C*). (*Insets*) Traces of the centroid of the bead image. (*D* and *E*) Histograms of the pausing times during rotation of V_1 in the presence of 10 μM (*D*) and 50 μM TBT-Cl (*E*). Black curve lines are fitted with a single exponential function, $y = C \times \exp(-t/\tau)$. Estimated time constant, τ, was shown on the figure and Table 1. The first bin is shown as gray bar. Blue lines show the result of a global fit for these two histograms with a time constant $\tau_{off} = 0.52 \pm 0.02$. Total counts of events were 1151 (5 molecules) (*D*) and 1400 (7 molecules) (*E*). (*F* and *G*) Histograms of the moving times during rotation in the presence of 10 μM (*F*) and 50 μM (*G*) TBT-Cl. A moving time was defined as a consecutive rotation time between neighboring pauses (>0.2 s). The lines are single exponential fits with $y = C \times \exp(-t/\tau)$. Total counts of events were 81 (5 molecules) (*F*) and 279 (7 molecules) (*G*). *C* and τ are a proportional constant and a time constant, respectively.

and therefore these events were not included in the fitting. A time constant obtained from this fitting was 0.04 ± 0.00 s (mean ± SE) (Fig. S1 *C*). This value was affected by long duration pauses, and therefore it might be calculated to be longer. The average occurrence of the short pause for ≤0.2 s events was 1.3 per revolution. This is comparable with the undefined pauses observed at 4 mM ATP in the absence of TBT-Cl. Therefore, the short pauses observed here were inherent, and those caused by TBT-Cl were determined to be those lasting >0.2 s. A curve calculated from the long pauses indicates that its time constant was 0.43 ± 0.04 s (mean ± SE) (Fig. 2 *D*). The first bin of the histogram (Fig. 2 *D, gray bar*), in which there are mixed events of pausing times, most of short pauses and short time portions of long pauses, was excluded from fitting for having little effect on a fit for long pauses. When the TBT-Cl concentration was increased to 50 μM TBT-Cl, V_1 apparently rotated stepwise, pausing at almost every 120° position (Fig. 2 *C*). Under this condition, two types of pauses were also observed and short and long time constants were obtained from the distribution of pauses. The average occurrence of short pause was 1.0 per revolution and the time constant was 0.05 ± 0.00 s (mean ± SE); this value was close to the undefined pauses (Fig. S1 *D*). The long time constant of 0.51 ± 0.03 s (mean ± SE) is close to the long time constant of 0.43 s at 10 μM TBT-Cl (Fig. 2 *E*). These results suggest that a long time constant is due to release of TBT-Cl from the enzyme. Furthermore, a global fit analysis was performed on these two histograms with a time constant, τ_{off} (Fig. 2, *D* and *E, blue lines*), which indicates that these two histograms are statistically the same.

Continuous time of the rotation between consecutive pauses due to the binding of TBT-Cl was analyzed to estimate k_{on} for TBT-Cl. To avoid the effect of undefined pauses, the short pauses (≤0.2 s) were excluded from this analysis. The histograms of rotating time at 10 and 50 μM TBT-Cl were fitted well with a single exponential (Fig. 2, *F* and *G*), suggesting that the binding of one TBT-Cl molecule is sufficient to make V_1 stop rotation and fall into pause. The estimated k_{on} was (1.4 ± 0.0) × 10^5 $M^{-1}s^{-1}$ (10 μM) and (1.0 ± 0.0) × 10^5 $M^{-1}s^{-1}$ (50 μM) (mean ± SE), and the dissociation constants, K_d, were deduced to be 16.6 μM and 19.6 μM, respectively (Table 1). These values are in the same range as is the K_i of 11.6 ± 0.7 μM estimated from the bulk-phase experiment illustrated in Fig. 1 *A*.

TBT-Cl inhibition at low ATP concentration

At 10 μM ATP, V_1 rotates stepwise, pausing at every 120° (Fig. 3 *A, red line* and *dots*). Under this condition, the dwell time for ATP binding to enzyme is the rate-limiting step.

TABLE 1 Kinetic parameters of the effect of TBT-Cl on V_1

ATP (μM)	TBT-Cl (μM)	τ_{off} (s)	τ_{on} (s)	k_{on} (10^5 $M^{-1}s^{-1}$)	K_d (μM)	τ_{ATP} (s)
4000	0	—	—	—	—	—
	10	0.43 ± 0.04	0.71 ± 0.02	1.4 ± 0.0	16.6	—
	50	0.51 ± 0.03	0.20 ± 0.01	1.0 ± 0.0	19.6	—
10	0	—	—	—	—	0.23 ± 0.01
	10	0.94 ± 0.8	—	—	—	(0.11 ± 0.01)

Each value was obtained from single-molecule measurements of V_1 under several conditions (mean ± SE). τ_{on} and τ_{off} are the time constants of TBT-Cl-bind and-release to/from V_1. The values were calculated from the histogram of moving times (τ_{on}) and pausing times (τ_{off}) (Figs. 2 and 3). K_d values were calculated from k_{off} /k_{on}. Dash means undetermined parameters.

The histogram was fitted well to a single exponential equation, giving a time constant τ_{ATP} of 0.23 ± 0.01 s (mean ± SE) (Fig. 3 *B, inset*), which is consistent with the previous report (27). In the presence of 10 μM TBT-Cl, the V_1-ATPase also rotated stepwise, pausing at every 120° interval (Fig. 3 *A, blue line* and *dots*). However, the rotation speed was much slower than that observed in the absence of TBT-Cl, as a consequence of the longer pauses. The frequency of events at a long time range increased in the presence of 10 μM TBT-Cl (Fig. 3 *C*). The histogram of this pausing time could be fitted well to the sum of two single exponentials, giving a short-τ value (τ_1) and a long-τ value (τ_2) (Fig. 3 *B*). The long-τ value of 0.94 ± 0.08 s (mean ± SE) was not observed in the absence TBT-Cl at 10 μM ATP. This value is close to the time constants observed in the presence of TBT-Cl at 4 mM ATP (Table 1), suggesting that release of TBT-Cl from the enzyme is responsible for the deduced long-τ value. On the other hand, the short-τ value of 0.11 ± 0.01, less than time bin-width size, was close to the τ_{ATP} value of 0.23 s determined in the absence of TBT-Cl. A global fit analysis represents long- and short-τ values as comparable with τ_{off} and τ_{ATP} (Fig. 3 *B*). These results indicate that the pauses observed in the presence of TBT-Cl at low ATP concentration are due to two independent events: 1) the ATP binding, and 2) the TBT-Cl release. This suggests that TBT-Cl has little effect on binding affinity for ATP.

Effect of TBT-Cl on step motions

To address the effect of TBT-Cl on the stepping motion of V_1, we measured the angular velocity for each step due to the TBT-Cl binding or the ATP binding (Fig. 4 *A*). At 10 μM ATP, the angular velocity of steps between consecutive durations due to the ATP binding dwell was calculated to be 69.4 ± 6.3 π rad s^{-1} (mean ± SE) (Fig. 4 *B*). In the presence of 50 μM TBT-Cl and 4 mM ATP, the observed pauses (>0.2 s) are primarily because of release of TBT-Cl from the enzyme (Fig. 2 *C*). The velocity for the 120° steps between the neighboring pauses (>0.2 s) was deduced to be 70.5 ± 8.3 π rad s^{-1} (mean ± SE). This is comparable to the velocity due to the ATP binding dwell. These results indicate that the binding of TBT-Cl to V_1 does not affect the rotational velocity between pauses.

TBT-Cl inhibition of $V_1\Delta F$ (A_3B_3D)

The rotor shaft in V_1 is comprised of the subunits D and F, which have no sequence homology to the γ and ε subunits of the rotor shaft in F_1. The subunit F has a structural similarity to the regulatory subunit CheY of the flagella motor, which regulates rotational direction in response to phosphorylation and dephosphorylation of its active site (28). This motif is well conserved in subunit F, suggesting that the subunit F might be the target of TBT-Cl. To test this possibility, we investigated the effect of TBT-Cl on A_3B_3D (referred to as $V_1\Delta F$), the minimum rotary unit in the V-ATPase (21). The ATPase activity of $V_1\Delta F$ obeyed simple Michaelis-Menten kinetics, and the Lineweaver-Burk plots shown in Fig. 5 *A* are consistent with noncompetitive inhibition as observed with V_1 (Fig. 1 *C*).

The apparent V_{max} values deduced from the plots were also decreased without any appreciable change in the K_m values. In the presence of 10 μM TBT-Cl, $V_1\Delta F$ rotates with frequent pauses such that the averaged rotation speed is much lower than that in the absence of TBT-Cl (Fig. 5 *B*). These results clearly indicate that ATPase activity of $V_1\Delta F$ was also noncompetitively inhibited by TBT-Cl, as with V_1, and the subunit F is not the target of TBT-Cl.

DISCUSSION

As observed with the F-ATPase, TBT-Cl inhibits the ATPase activity of the V-ATPase. Ueno et al. found that TBT-Cl decreased the rotation rate of the γ subunit within TF_oF_1, the ATP synthase from thermophilic *Bacillus* PS3, but it had no effect on rotation of the γ subunit in isolated F_1 (20). We demonstrated in this study that preincubation of the V_o-liposome with TBT-Cl completely abolishes proton permeability (Fig. 1 *B*). In *T.thermophilus* V-ATPases, subunit V_o-a complexed with the proteolipid ring comprises the proton channel and shows proton permeability (12). Although *T.thermophilus* V_o-a showed no sequence homology to the subunit a in F_o, several lines of evidence suggest that the proton channel in the *T.thermophilus* V_o has a structure similar to that of the F_o proton channel (29). It seems likely that TBT-Cl interacts with the *T.thermophilus* V_o channel and F_o channel in a similar manner. It is noted that the eukaryotic V_o domain appeared considerably different from that of prokaryotic counterparts; it contains hydrophilic stator subunits and a hetero-oligomeric rotor ring, and it shows no proton permeability when V_1 domain dissociates from V_o domain (4). Further study is necessary to clarify

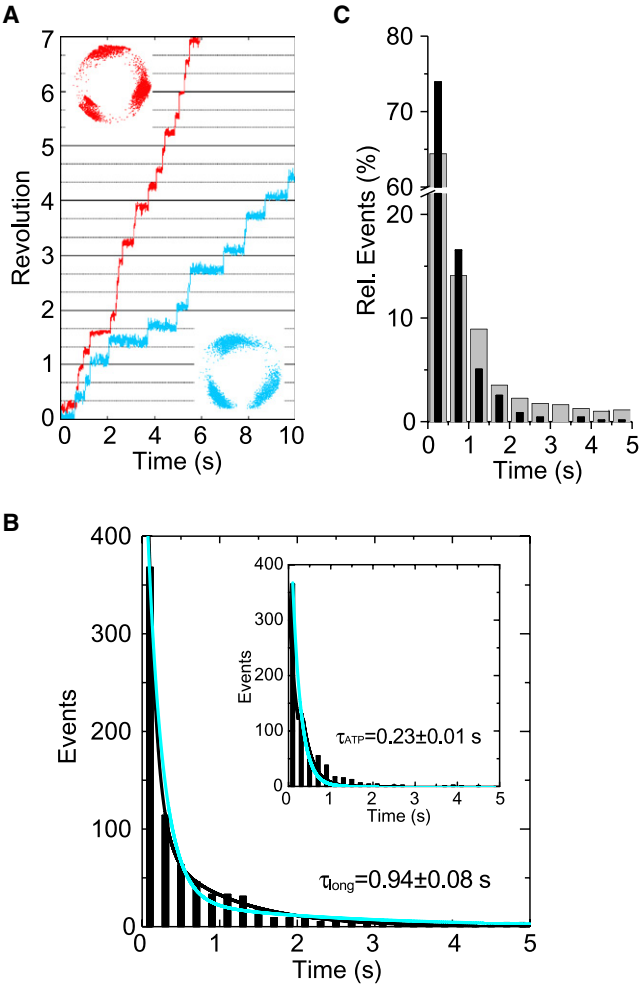

FIGURE 3 Effect of TBT-Cl on the rotation of V_1 at a low ATP concentration. (*A*) Time courses of rotation in the absence (*red line* and *dots*) and presence (*blue line and dots*) of 10 μM TBT-Cl. (*Inset*) Traces of the centroid of the bead images. (*B*) Histogram of pausing time at 10 μM ATP in the presence of 10 μM TBT-Cl. It was fitted with sum of two exponential, $y = C_1 \times \exp(-t/\tau_1) + C_2 \times \exp(-t/\tau_2)$ ($\tau_1 < \tau_2$). Estimated time constants, shown on the figure and in Table 1. (τ_1 value was calculated to be 0.11 $\pm$ 0.01, which was below the bin width.) Total counts of events were 713 (8 molecules). (*Inset*) Histogram of pausing time at 10 μM ATP with no TBT-Cl. The line is fit with $y = C \times \exp(-t/\tau_{ATP})$. Total counts of events were 795 (9 molecules). Blue lines show the result of a global fit for these two histograms with time constants $\tau_{ATP} = 0.20 \pm 0.01$ and $\tau_{off} = 2.16 \pm 1.03$. (*C*) Frequency of pausing time at 10 μM ATP with no TBT-Cl (*black bar*) and 10 μM TBT-Cl (*gray bar*).

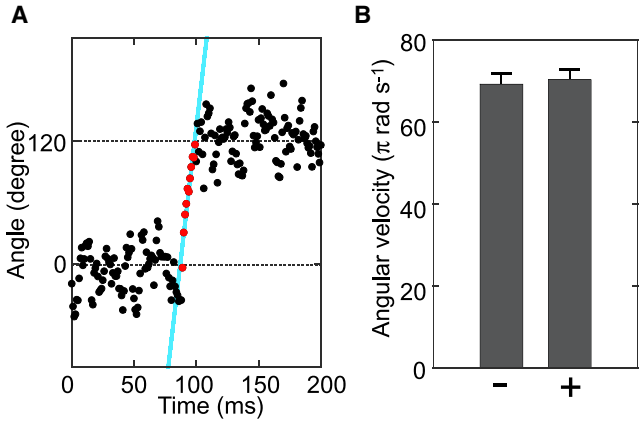

FIGURE 4 Angular velocity of step motion in the presence of TBT-Cl. (*A*) Magnification of step at 4 mM ATP in the presence of 50 μM TBT-Cl. Steps distinguished from pauses are fitted with linear segments to estimate the average angular velocity. (*B*) The angular velocity of the single 120° step motion at 10 μM ATP in the absence of TBT-Cl (−) and at 4 mM ATP in the presence of 50 μM TBT-Cl (+). Each velocity was calculated from 25 steps for 5 molecules.

inhibitory effects of TBT on the function of eukaryotic V_o domain. Binding of TBT-Cl to the V_o channel led to nearly complete inhibition of the ATPase activity of the holoenzyme. Also, unlike F_1, the ATPase activity of V_1 was dramatically inhibited with TBT-Cl in the micromolar range. Bulk-phase experiments indicated that TBT-Cl binds to V_1 noncovalently and inhibits its ATPase activity noncompetitively (Fig. 1). Because the ATPase activity of $V_1\Delta F$ was also inhibited, subunit F is not the target of TBT-Cl (Fig. 5). The catalytic A subunit is homologous to the F_1-β subunit (13); however, subunit A contains nonhomologous regions, which could be the target of TBT-Cl. Further studies are necessary to identify the binding site for TBT-Cl on V_1. Our results clearly indicate that TBT-Cl binds to the V_1 domain in addition to the V_o domain, and it inhibits the activity of holoenzyme V-ATPase. This is the first report to demonstrate that TBT-Cl can inhibit V_1 holoenzyme in a noncompetitive manner.

We also examined the inhibition mechanism of V_1 by TBT-Cl using single-molecule imaging techniques. TBT-Cl apparently decreased the averaged rotational rate of V_1 and imposed stepwise rotation on V_1, even at saturating ATP concentration. Analysis of the pausing time in the presence of TBT-Cl indicated that each pause was caused by the binding of one TBT-Cl molecule to the enzyme (Fig. 2). Pauses caused by TBT-Cl were also observed at low ATP concentrations, in which V_1 rotates stepwise due to the ATP binding dwell. Under this condition, V_1 paused at each 120° dwell position (Fig. 3). Two time-rate constants were deduced from the dwell-time analysis. As summarized in Table 1, the short-τ value in the presence of TBT-Cl is comparable to the τ value due to ATP binding events. On the other hand, the long-τ value at low ATP concentration is close to the τ value due to the events of TBT-Cl binding at saturating ATP concentration. These results indicate that the ATP binding and TBT-Cl binding events occur mostly at the same dwell position but are independent of each other, which is consistent with the bulk-phase analysis. We recently demonstrated that the dwell for the ATP binding is the same as or very close to the catalytic dwell where ATP hydrolysis or product release takes place (22). In contrast, single-molecule analysis of F_1 revealed that 120° step consists of 80° substep driven by ATP binding and 40° substep by product release (30,31). From the single-molecule analyses of V_1, it is concluded that TBT-Cl inhibits the catalytic event(s) but

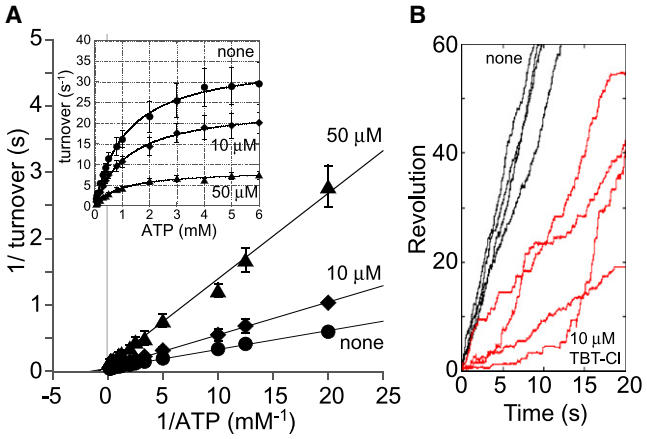

FIGURE 5 Effect of TBT-Cl on ATPase activity and rotation of $V_1\Delta F$. (*A*) Lineweaver-Burkplots representing reciprocal of the $V_1\Delta F$ ATPase activity versus reciprocal of ATP concentrations in the presence of 50 μM (▲) and 10 μM (◆), and in the absence of TBT-Cl (●). The graphics in the plots portray the consequences of noncompetitive inhibition. The plots are fitted by linear regression on full data sets. (*Inset*) [S]-*v* plots derived from the Lineweaver-Burk plots. The lines show fitting functions with $V_{max} = 8.6 \pm 1.7\ s^{-1}$ and $K_m = 1.0 \pm 0.1$ mM (50 μM TBT-Cl), $V_{max} = 24.4 \pm 6.4\ s^{-1}$ and $K_m = 1.2 \pm 0.2$ mM (10 μM TBT-Cl), and $V_{max} = 35.7 \pm 11.1\ s^{-1}$ and $K_m = 1.2 \pm 1.2$ mM (no TBT-Cl), respectivly. Each point represents mean ± SE of three measurements. (*B*) Time course of the rotation of $V_1\Delta F$ in the presence of 10 μM (*red line*) and in the absence of TBT-Cl (*black line*).

does not alter the binding affinity for ATP in the mechanochemical cycle of V_1.

Our results demonstrate that TBT-Cl inhibits a specific event in the mechanochemical cycle catalyzed by the V_1 motor. This new finding provides a basis for designing new experiments to unravel details of the rotary catalysis by V_1. For example, a crystal structure of V_1 containing both bound ATP and TBT-Cl would provide a snapshot of the rotary motor in which the 120° rotational step had just completed.

SUPPORTING MATERIAL

One figure is available at http://www.biophysj.org/biophysj/supplemental/S0006-3495(08)00105-7.

We thank our colleagues, especially Drs. H. Imamura, E. Muneyuki, H. Ueno, T. Masaike, T. Nishizaka, Y. Hirono-Hara, F. Motojima, and T. Yano, for critical discussions. We also thank E. Saita, M. Nakano, M. Belz, T. Murakami-Fuse, and S. Funamoto for their technical advice. We are grateful to R. Yasuda and K. Adachi for programming the custom software.

This work was partly supported by Grants-in-Aid from the Ministry of Education, Science, Sports and Culture of Japan (Nos. 1837005, 18657041, and 19042008) and a target proteins research program (B-37, to KY).

REFERENCES

1. Fent, K., and W. Meier. 1992. Tributyltin-induced effects on early life stages of minnows *Phoxinus phoxinus*. *Arch. Environ. Contam. Toxicol.* 22:428–438.
2. Shimasaki, Y., T. Kitano, Y. Oshima, S. Inoue, N. Imada, et al. 2003. Tributyltin causes masculinization in fish. *Environ. Toxicol. Chem.* 22:141–144.
3. Nishi, T., and M. Forgac. 2002. The vacuolar H^+-ATPases—nature's most versatile proton pumps. *Nat. Rev. Mol. Cell Biol.* 3:94–103.
4. Hughes, G., M. A. Harrison, Y. I. Kim, D. E. Griffiths, M. E. Finbow, et al. 1996. Interaction of dibutyltin-3-hydroxyflavone bromide with the 16 kDa proteolipid indicates the disposition of proton translocation sites of the vacuolar ATPase. *Biochem. J.* 317:425–431.
5. Apps, D. K., and L. C. Webster. 1996. Interaction of organotins with a vacuolar-type H^+-ATPase. *Biochem. Biophys. Res. Commun.* 227:839–845.
6. Shimizu, S., T. Imanaka, T. Takano, and S. Ohkuma. 1992. Major ATPases on clofibrate-induced rat liver peroxisomes are not associated with 70 kDa peroxisomal membrane protein (PMP70). *J. Biochem. (Tokyo).* 112:376–384.
7. Kakinuma, Y., and K. Igarashi. 1994. Purification and characterization of the catalytic moiety of vacuolar-type Na^+-ATPase from *Enterococcus hirae*. *J. Biochem. (Tokyo).* 116:1302–1308.
8. Yokoyama, K., E. Muneyuki, T. Amano, S. Mizutani, M. Yoshida, et al. 1998. V-ATPase of *Thermus thermophilus* is inactivated during ATP hydrolysis but can synthesize ATP*. *J. Biol. Chem.* 273:20504–20510.
9. Imamura, H., M. Nakano, H. Noji, E. Muneyuki, S. Ohkuma, et al. 2003. Evidence for rotation of V_1-ATPase. *Proc. Natl. Acad. Sci. USA.* 100:2312–2315.
10. Yokoyama, K., M. Nakano, H. Imamura, M. Yoshida, and M. Tamakoshi. 2003. Rotation of the proteolipid ring in the V-ATPase. *J. Biol. Chem.* 278:24255–24258.
11. Yokoyama, K., Y. Akabane, N. Ishii, and M. Yoshida. 1994. Isolation of prokaryotic V_oV_1-ATPase from a thermophilic eubacterium *Thermus thermophilus*. *J. Biol. Chem.* 269:12248–12253.
12. Yokoyama, K., S. Ohkuma, H. Taguchi, T. Yasunaga, T. Wakabayashi, et al. 2000. V-Type H^+-ATPase/synthase from a thermophilic eubacterium, *Thermus thermophilus*. Subunit structure and operon. *J. Biol. Chem.* 275:13955–13961.
13. Tsutsumi, S., K. Denda, K. Yokoyama, T. Oshima, T. Date, et al. 1991. Molecular cloning of genes encoding major two subunits of a eubacterial V-type ATPase from *Thermus thermophilus*. *Biochim. Biophys. Acta.* 1098:13–20.
14. Yokoyama, K., K. Nagata, H. Imamura, S. Ohkuma, M. Yoshida, et al. 2003. Subunit arrangement in V-ATPase from *Thermus thermophilus*. *J. Biol. Chem.* 278:42686–42691.
15. Bowman, E. J., L. A. Graham, T. H. Stevens, and B. J. Bowman. 2004. The bafilomycin/concanamycin binding site in subunit c of the V-ATPases from *Neurospora crassa* and *Saccharomyces cerevisiae*. *J. Biol. Chem.* 279:33131–33138.
16. Boya, P., R. A. Gonzalez-Polo, N. Casares, J. L. Perfettini, P. Dessen, et al. 2005. Inhibition of macroautophagy triggers apoptosis. *Mol. Cell. Biol.* 25:1025–1040.
17. Tanigaki, K., S. Sasaki, and S. Ohkuma. 2003. In bafilomycin A_1-resistant cells, bafilomycin A_1 raised lysosomal pH and both prodigiosins and concanamycin A inhibited growth through apoptosis. *FEBS Lett.* 537:79–84.
18. Wang, Y., T. Inoue, and M. Forgac. 2005. Subunit a of the yeast V-ATPase participates in binding of bafilomycin. *J. Biol. Chem.* 280:40481–40488.
19. von Ballmoos, C., J. Brunner, and P. Dimroth. 2004. The ion channel of F-ATP synthase is the target of toxic organotin compounds. *Proc. Natl. Acad. Sci. USA.* 101:11239–11244.
20. Ueno, H., T. Suzuki, K. Kinosita, Jr., and M. Yoshida. 2005. ATP-driven stepwise rotation of F_oF_1-ATP synthase. *Proc. Natl. Acad. Sci. USA.* 102:1333–1338.
21. Imamura, H., C. Ikeda, M. Yoshida, and K. Yokoyama. 2004. The F subunit of *Thermus thermophilus* V_1-ATPase promotes ATPase activity but is not necessary for rotation. *J. Biol. Chem.* 279:18085–18090.
22. Imamura, H., M. Takeda, S. Funamoto, K. Shimabukuro, M. Yoshida, et al. 2005. Rotation scheme of V_1-motor is different from that of F_1-motor. *Proc. Natl. Acad. Sci. USA.* 102:17929–17933.

23. Noji, H., R. Yasuda, M. Yoshida, and K. Kinosita, Jr.. 1997. Direct observation of the rotation of F_1-ATPase. *Nature*. 386:299–302.

24. Matsuya, H., M. Okamoto, T. Ochi, A. Nishikawa, S. Shimizu, et al. 2000. Reversible and potent uncoupling of hog gastric $H^+ + K^+$-ATPase by prodigiosins. *Biochem. Pharmacol*. 60:1855–1863.

25. Yasuda, R., H. Noji, K. Kinosita, Jr., and M. Yoshida. 1998. F_1-ATPase is a highly efficient molecular motor that rotates with discrete 120 degree steps. *Cell*. 93:1117–1124.

26. Hirono-Hara, Y., H. Noji, M. Nishiura, E. Muneyuki, K. Y. Hara, et al. 2001. Pause and rotation of F_1-ATPase during catalysis. *Proc. Natl. Acad. Sci. USA*. 98:13649–13654.

27. Yasuda, R., H. Noji, M. Yoshida, K. Kinosita, Jr., and H. Itoh. 2001. Resolution of distinct rotational substeps by submillisecond kinetic analysis of F_1-ATPase. *Nature*. 410:898–904.

28. Makyio, H., R. Iino, C. Ikeda, H. Imamura, M. Tamakoshi, et al. 2005. Structure of a central stalk subunit F of prokaryotic V-type ATPase/synthase from *Thermus thermophilus*. *EMBO J*. 24:3974–3983.

29. Kawasaki-Nishi, S., T. Nishi, and M. Forgac. 2001. Arg-735 of the 100-kDa subunit a of the yeast V-ATPase is essential for proton translocation. *Proc. Natl. Acad. Sci. USA*. 98:12397–12402.

30. Shimabukuro, K., R. Yasuda, E. Muneyuki, K. Y. Hara, K. Kinosita, Jr., et al. 2003. Catalysis and rotation of F_1 motor: cleavage of ATP at the catalytic site occurs in 1 ms before 40 degree substep rotation. *Proc. Natl. Acad. Sci. USA*. 100:14731–14736.

31. Adachi, K., K. Oiwa, T. Nishizaka, S. Furuike, H. Noji, et al. 2007. Coupling of rotation and catalysis in F_1-ATPase revealed by single-molecule imaging and manipulation. *Cell*. 130:309–321.